Available online at www.sciencedirect.com

ScienceDirect

Geochimica et Cosmochimica Acta 260 (2019) 49–61

Geochimica et Cosmochimica Acta

www.elsevier.com/locate/gca

Large benthic fluxes of dissolved iron in China coastal seas revealed by $^{224}Ra/^{228}Th$ disequilibria

Xiangming Shi [a,b], Lin Wei [a,b], Qingquan Hong [a,b], Lingfeng Liu [c], Yuning Wang [a,b] Xueying Shi [a,b], Ying Ye [d], Pinghe Cai [a,b,*]

[a] State Key Laboratory of Marine Environmental Science, Xiamen University, Xiamen 361005, PR China
[b] College of Ocean and Earth Sciences, Xiamen University, Xiamen 361005, PR China
[c] Shanwei Marine Environmental Monitoring Center Station, State Oceanic Administration, Shanwei 516600, PR China
[d] Alfred Wegener Institute for Polar and Marine Research, Bremerhaven 27515, Germany

Received 6 December 2018; accepted in revised form 17 June 2019; Available online 22 June 2019

Abstract

We report benthic flux estimates of Fe from China coastal seas based on a recently developed $^{224}Ra/^{228}Th$ disequilibrium approach. There were considerable temporal and spatial variabilities in benthic Fe fluxes, which spanned over 4–5 orders of magnitude, from <10 μmol m^{-2} d^{-1} up to ~100 mmol m^{-2} d^{-1}. Nonetheless, we have identified a prominent trend in China coastal seas showing that benthic Fe fluxes tended to decline exponentially with bottom depth. This trend is probably a result of kinetic energy and chemically bound energy gradients that culminate in the coastal seas. In the meantime, large benthic Fe fluxes were more frequently observed within a narrow redox window of 100–150 μM dissolved oxygen (DO) in the bottom water. This observation contradicts an early assumption that iron release from continental margin sediments increases with decreasing DO concentration in the bottom water. It possibly reflects a compromise of oxygen-demanded irrigation that acts to enhance Fe release from bottom sediments, and re-oxidation of dissolved Fe(II) that results in more efficient Fe retention near the sediment-water interface. Notably, benthic fluxes of Fe based on $^{224}Ra/^{228}Th$ disequilibria were one order of magnitude larger than those derived from the porewater concentration gradient method. Moreover, the isotopic estimates were >30 times higher than the historical measurements based on the traditional incubation method (i.e., the benthic chamber method) in other coastal seas. However, our estimates of benthic Fe flux were in general agreement with the reported flux value based on a new two dimensional imaging technique.

Keywords: Benthic flux; Dissolved Fe; $^{224}Ra/^{228}Th$ disequilibria; Porewater exchange; China coastal seas

1. INTRODUCTION

Dissolved iron (Fe) plays a pivotal role in regulating biological productivity and carbon export over large areas of the surface ocean (Martin and Gordon, 1988; Boyd and Ellwood, 2010). Low Fe concentrations are believed to limit nitrogen fixation and photosynthesis in half of the world ocean (Kolber et al., 1994; Moore et al., 2009). Changes in Fe supply to the ocean are suggested to be an important driver for the glacial/interglacial cycles in atmospheric carbon dioxide concentration in the geological past (Martin, 1990; de Baar et al., 1995; Sigman and Boyle, 2000). In this context, there is a pressing need to constrain Fe sources so as to understand the biogeochemical cycle of Fe and its impact on the carbon cycling in the ocean.

* Corresponding author at: State Key Laboratory of Marine Environmental Science, Xiamen University, Xiamen 361005, PR China. Fax: +86 592 2180655.
E-mail address: Caiph@xmu.edu.cn (P. Cai).

https://doi.org/10.1016/j.gca.2019.06.026
0016-7037/

Coastal sediments represent a potentially important source of Fe to the upper ocean (Lam and Bishop, 2008; Jeandel et al., 2011; Conway and John, 2014). However, it is a major challenge in marine chemistry to accurately quantify Fe flux from coastal sediments. Previous estimates of the benthic flux of Fe were derived either from porewater concentration profiles (Shaw et al., 1990), or from incubation experiments using a benthic chamber (Elrod et al., 2004). The porewater concentration gradient method does not take into account a major mechanism for solute transfer across the sediment-water interface, i.e., irrigation (Aller, 1980a). The deployment of a benthic chamber inevitably interferes with the flow field and changes the redox conditions near the seafloor. Consequently, artificial biases may exist in these benthic Fe flux estimates (Severmann et al., 2010; Homoky et al., 2012). This is particularly an issue in coastal seas that are characterized by strong tides, waves, shear flows, and intense activities of benthic fauna (Huettel et al., 2014; Thibault de Chanvalon et al., 2017). As such, new tools need to be invoked for better quantification of benthic Fe fluxes.

Here we report benthic fluxes of Fe in China coastal seas based on a recently developed method – the $^{224}Ra/^{228}Th$ disequilibrium approach (Cai et al., 2014, 2015). In marine sediments, ^{224}Ra (half-life = 3.66 days) is continuously produced via alpha decay from ^{228}Th (half-life = 1.91 years). Unlike its highly particle-reactive parent, an appreciable fraction of ^{224}Ra in sediment particles can be released into saline interstitial water. By virtue of a variety of processes operating near the seafloor, such as irrigation and shear flow-induced advective transport (Berner, 1980; Huettel et al., 2014), some soluble ^{224}Ra ultimately migrates across the sediment-water interface into the overlying water. This flux of ^{224}Ra can be readily quantified from the deficit of ^{224}Ra relative to ^{228}Th in the near-surface sediment. In combination with the ratio of the concentration gradients at the sediment-water interface, i.e., ^{224}Ra concentration gradient divided by the component concentration gradient, the ^{224}Ra flux is converted into a flux estimate of the component of interest. This method integrates benthic flux events over a time scale of ~1–10 days prior to sampling. In contrast to the traditional incubation method, a major advantage of the $^{224}Ra/^{228}Th$ disequilibrium method is that it does not impose any interference to the system.

2. SAMPLING OVERVIEW AND METHODS

2.1. Study regions

Samples were collected from four distinct coastal settings: (1) the northern South China Sea shelf and the adjacent Pearl River Estuary, (2) the Jiulong River Estuary, (3) the inner shelf of the East China Sea adjacent to the Yangtze River Estuary, and (4) the Yellow Sea and Bohai Sea (Fig. 1). These settings cover a diversity of typical coastal biogeochemical provinces in China coastal seas, changing from subtropical to temperate zones, and from estuaries to inner continental shelves. The dominant benthos of the seas are polychaetes, mollusks and crustacea, and their abundances are of considerably temporal and spatial variabilities (He et al., 1988; Li et al., 2010; Liu et al., 2014). Bottom water was collected ~1–2 m above the seafloor with Niskin bottles and sediments were taken from a standard box corer (30 × 30 × 60 cm). It should be noted that our sampling was technically confined within the inner continental shelves where the seafloors are commonly dominated by fine-grained ($\phi = 2.4$–6.6) sediments.

2.2. ^{224}Ra and ^{228}Th analyses

After ensuring that the sediment interface in the box corer was intact, sediment sub-cores were collected by inserting polycarbonate tubes into the bulk sediment core. A sediment sub-core was sliced into 1-cm thick slabs immediately after sample collection. De-ionized water was added to the sediment slabs to form a slurry in a Teflon beaker. Subsequently, concentrated $NH_3{\cdot}H_2O$, $KMnO_4$ (8.0 g L^{-1}) and $MnCl_2$ (3.0 g $MnCl_2{\cdot}4H_2O$ L^{-1}) solutions (reagent grade) were added to form a suspension of MnO_2. The MnO_2 suspension and the sediment with absorbed ^{224}Ra and ^{228}Th were filtered onto a 142-mm 0.7 μm (nominal pore size) glass microfiber filter (GFF/Whatman®). The filter was placed into a holder specified for sediment samples and counted for 4–6 h in a delayed coincidence counting system (the RaDeCC system). About 8–10 days later, the sample was re-counted using the same RaDeCC system. The activities of bulk sediment ^{224}Ra and ^{228}Th were calculated from the two measurements. In order to verify the performance of the system, a third measurement was conducted ~25 days after sample collection. The counting efficiency for sediment samples was determined with a ^{232}U-^{228}Th standard using the method of standard addition. The reproducibility of ^{224}Ra and ^{228}Th measurements in bulk sediments based on this method has been improved to a level of ±3–4%, compared to ±5–7% at its developing stage (Cai et al., 2012; Hong et al., 2018a).

Porewater was extracted from three parallel sediment sub-cores by inserting an array of Rhizon samplers directly into the sediment (Seeberg-Elverfeldt et al., 2005). Approximately 20 mL of porewater was retrieved at discrete depths in the upper 0–20 cm sediment layer. The porewater samples for ^{224}Ra analyses were transferred into a 250 mL Teflon beaker and 100 mL of de-ionized water was added. With addition of concentrated $NH_3{\cdot}H_2O$, the pH was adjusted to 8.0–9.0. Subsequently, $KMnO_4$ and $MnCl_2$ solutions were added to form a suspension of MnO_2, which was then filtered onto a 142-mm 0.7 μm GFF filter and counted for ~10 h in the RaDeCC system. For the analyses of dissolved ^{224}Ra in the bottom water, an aliquot of 4 L seawater was collected using Niskin bottles. After filtration, ^{224}Ra activity in the filtrate was determined in a manner similar to the measurement of porewater ^{224}Ra. The counting efficiency of the RaDeCC system for dissolved ^{224}Ra samples was determined with a ^{232}U-^{228}Th standard that was prepared in the same manner with the porewater samples. The uncertainty associated with porewater and bottom water ^{224}Ra measurements was about ±10% (Cai et al., 2015).

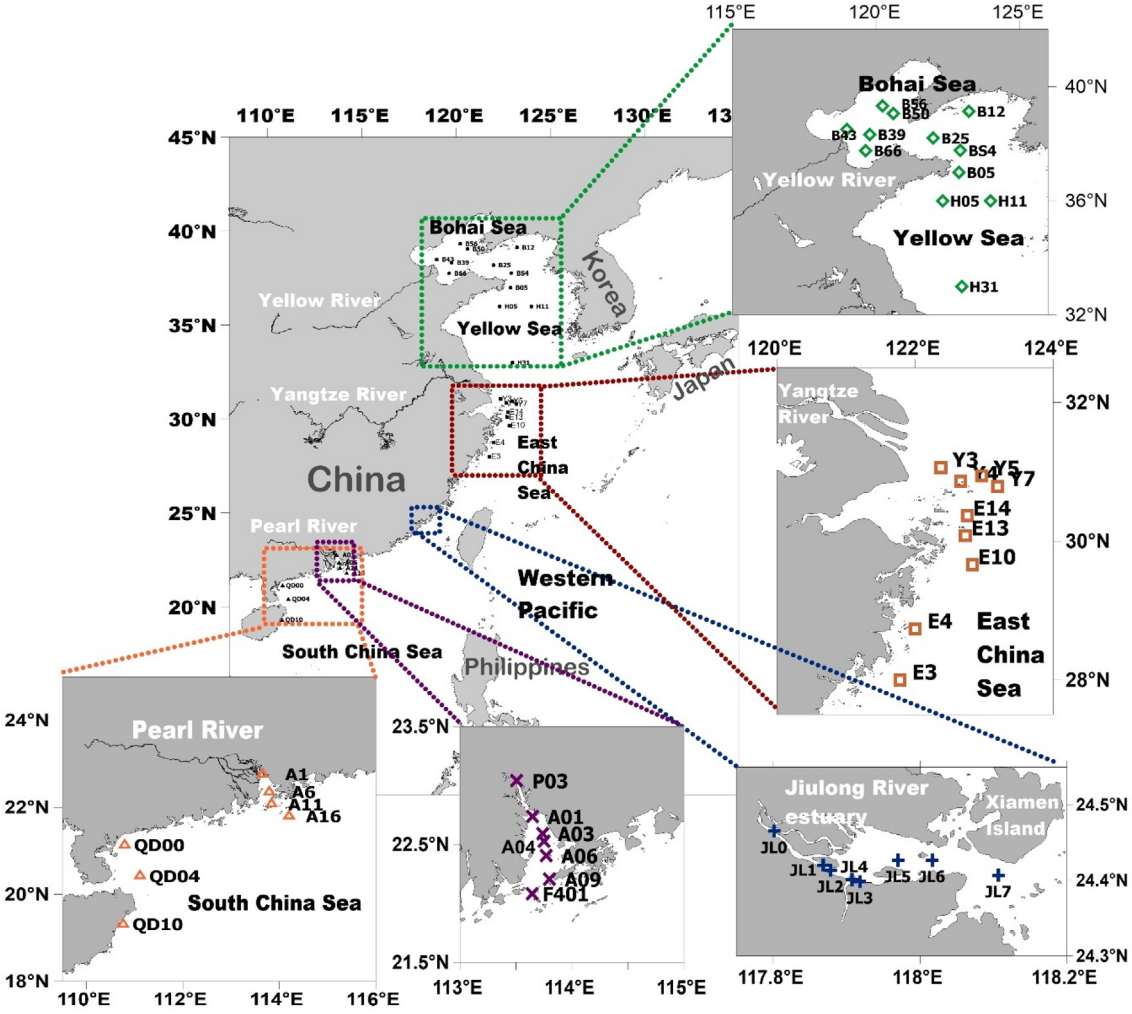

Fig. 1. Location of benthic Fe flux measurements in the China coastal seas. The inset maps show the location of sampling sites in the northern South China Sea shelf and the adjacent Pearl River Estuary (lower left panel), the Pearl River Estuary (lower middle panel), the Jiulong River Estuary (lower right panel), the East China Sea shelf adjacent to the Yangtze River Estuary (middle panel), the Yellow Sea and the Bohai Sea (upper panel).

2.3. Dissolved Fe analyses

Porewater was collected with acid-cleaned Rhizon samplers (filtration cut-off of 0.1 μm) at sediment depths of 0.5, 1.5, 2.5, 3.5, 4.5, 5.5, 7.5, 9.5, 11.5, and 14.5 cm. The samplers were pre-cleaned in order of 48 h 2 M HCl (reagent grade) and 48 h 0.5 M HCl (Fisher Scientific Optima), and rinsed with 18.2 mΩ de-ionized water. A 5–6 mL aliquot of porewater was extracted at each sediment depth from a sediment sub-core and then was acidified to pH < 2 with 65% quartz-distilled HNO_3 (5 μL per mL of porewater) in a clean van onboard. During each cruise, several blanks were prepared from de-ionized water onboard following the same sampling procedure. In a land-based clean lab (100-class), the samples were diluted 10–100 fold with a 2% quartz-distilled HNO_3 solution containing 5 ng g^{-1} Re, Rh, Sc, and Be as internal standards. A succession of external calibration standards was prepared from certified stock solutions. Analyses of diluted samples and blanks were performed on an Agilent 7700 quadrupole ICP-MS equipped with a collision-reaction cell. Internal standard Sc was monitored throughout the measurements and used to correct for the change in Fe signal intensity over time. Triplicate procedural determinations were performed on selected samples and the mean deviation of analyses was typically within 5%. Mean procedural blanks for sampling and analyses were 66 ± 3 nmol L^{-1} (n = 8, 1 s.d.). It should be noted that our samples are sediment porewaters with Fe concentrations generally >1 μmol L^{-1}, far beyond the detection limit of the method. As such, any errors introduced by potential contamination in the process of sample collection and analysis must be negligible.

2.4. Ancillary analyses

Dissolved oxygen (DO) in the bottom water was measured onboard using the Winkler titration method, which typically has an uncertainty of ±1 μM. Temperature and

salinity data were derived directly from a CTD meter attached on the rosette sampler. For the analyses of porosity, separate sediment subsamples were dried in an oven at 60 °C for 24 h. The porosity was calculated from the weight loss using a grain density of 2.6 g cm^{-3}.

3. RESULTS

3.1. Distributions of ^{224}Ra and ^{228}Th in sediments

Data sets of ^{224}Ra and ^{228}Th activities in bulk sediments, as well as dissolved ^{224}Ra activities in porewater are presented in Tables S1–S3. Typical depth profiles of ^{224}Ra and ^{228}Th in the near-surface sediment are shown in Fig. 2. Activities of ^{228}Th were generally high in the topmost sediment, and decreased to a relatively low level of ~0.5–1 dpm g^{-1} below depths of ~5 cm. The highest ^{228}Th activity (5.26 ± 0.18 dpm g^{-1}) was observed at St. H05 in the Yellow Sea. As the daughter of ^{228}Th, ^{224}Ra had similar distribution patterns. Nonetheless, significant deficit of ^{224}Ra relative to ^{228}Th ($^{224}Ra/^{228}Th < 0.9$, $p < 0.05$ by T-Test) in the upper 0–5 cm sediment was commonly observed at most of our sampling sites. As shown in Fig. 2, ^{224}Ra deficit can be evident down to a depth of ~12 cm (e.g., St. A1), indicating active migration of ^{224}Ra out of the near-surface sediment into the overlying water column at these locations. Below 10 cm, the activity ratio (AR) of $^{224}Ra/^{228}Th$ was generally indiscernible from unity. This implies that effective benthic solute exchange is mostly confined within the near-surface sediment.

Porewater ^{224}Ra activities ranged from 5.6 ± 0.5 dpm L^{-1} to 71.6 ± 6.2 dpm L^{-1}, about 1–2 orders

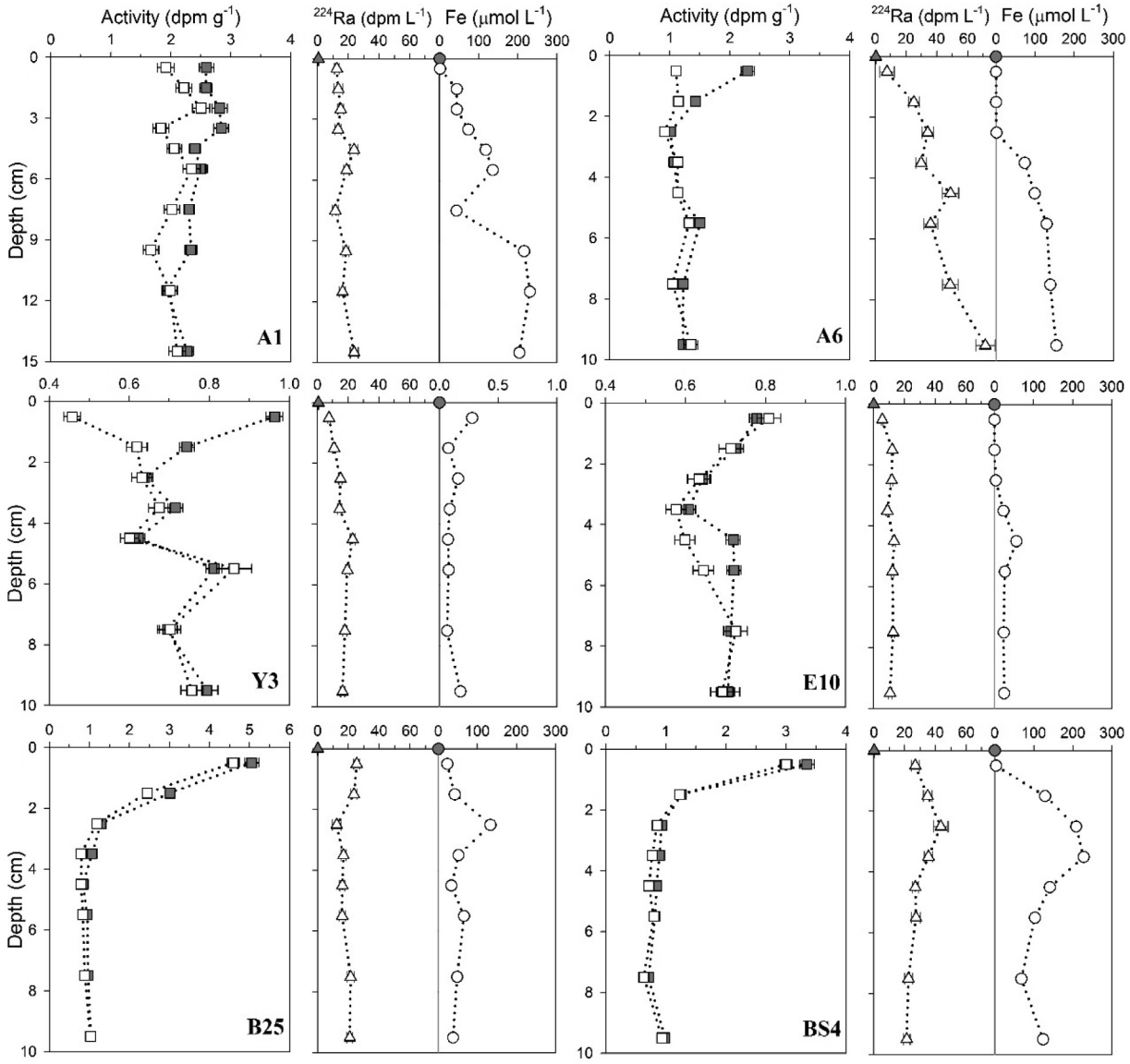

Fig. 2. Typical profiles of total ^{224}Ra (open square) and ^{228}Th (solid square), dissolved ^{224}Ra (open triangle) and dissolved Fe (open circle) in the upper sediment column. The solid symbols stand for the component concentrations in the overlying water. Note that the scales of x- and y-axis may not be identical. Error bars ($\pm 1\sigma$) were shown only for ^{224}Ra and ^{228}Th data.

of magnitude higher than those in the overlying water (<0.02–0.60 dpm L^{-1}, Tables S1–S3). Thus, sharp gradients of dissolved ^{224}Ra were commonly observed near the sediment-water interface (Table 1). Nonetheless, porewater ^{224}Ra activities were relatively constant at a specific site, and the depth variation was generally in the vicinity of ±10%.

3.2. Fe concentration in porewater

All dissolved Fe data in porewater are exhibited in Tables S1–S5. Typical depth profiles are shown in Fig. 2. Compared to dissolved ^{224}Ra, Fe concentrations were much more variable in porewater. Overall, dissolved Fe concentrations in porewater were relatively high (>100 μmol L^{-1}) in the inner estuaries as compared to the shelves (<50 μmol L^{-1}). In the uppermost sediment, porewater Fe concentration was generally low (<10 μmol L^{-1}). Below the surficial sediment, it increased sharply with depth and could even reach a level of >1500 μmol L^{-1} (see Table S4). This pattern may be a result of redox transformation between Fe species in sediments: microbial reduction of Fe oxides bound onto sediment particles resulted in the release of more soluble Fe(II) in the deeper sediment; with upward migration of dissolved Fe, the exposure to the overlying oxic seawater could lead to re-oxidization of dissolved Fe(II) to Fe oxides, which may then be re-bound onto sediment particles via precipitation (Aller, 1980a).

4. DISCUSSION

4.1. Estimation of benthic Fe fluxes

We calculate the benthic flux of ^{224}Ra by integrating the ^{224}Ra deficit from the sediment surface to the sampling depth, or to a depth (z) below which total ^{224}Ra and ^{228}Th were constantly in secular equilibrium (Cai et al., 2014):

$$F_{Ra} = \lambda_{Ra} \int_0^z (A_{Th} - A_{Ra})dz \quad (1)$$

where F_{Ra} represents benthic flux of ^{224}Ra, λ_{Ra} is the decay constant of ^{224}Ra (0.189 d^{-1}), A_{Th} and A_{Ra} denote activities of ^{228}Th and ^{224}Ra in the bulk sediment (sediment particulate + porewater), respectively. A positive value stands for upward flux out of sediments. All ^{224}Ra flux estimates are shown in Table 1. It should be emphasized that the negative flux values presented in Table 1 are, within uncertainty (±2σ), indiscernible from zero. Overall, the most marked deficit of total ^{224}Ra in the sediment column occurred within the estuaries. In contrast, the depletion of total ^{224}Ra was less pronounced over the continental shelves. Consequently, benthic flux of ^{224}Ra generally decreased with distance offshore.

In combination with measurements of the ratio of the concentration gradients of component/^{224}Ra at the sediment-water interface, the ^{224}Ra flux is converted into a flux estimate of the objective component (i.e., Fe in this case) using the following expression (Cai et al., 2014):

$$F_{Fe} = F_{Ra} \cdot \frac{D_S^{Fe}}{D_S^{Ra}} \cdot \frac{\frac{\partial Fe}{\partial z}}{\frac{\partial Ra}{\partial z}} \quad (2)$$

where $\frac{\partial Fe}{\partial z}$ and $\frac{\partial Ra}{\partial z}$ are the concentration gradients of dissolved Fe and ^{224}Ra at the sediment-water interface, respectively. The term D_S^{Fe}/D_S^{Ra} represents the ratio of the molecular diffusion coefficients of Fe and ^{224}Ra in sediments, and is identical to the ratio (0.80) in seawater. Moreover, it remains fairly constant over a temperature range of 0–25 °C (Schulz, 2006). Note that while only the diffusion coefficients for Ra and the objective component are included in Eq. (2), this does not mean that advective transport is unimportant. Rather, it assumes that diffusion is the rate-limiting step for solute exchange between sediments and ambient waters. Strong advective flow with length scales of several centimeters could take place within the burrows of benthic fauna in cohesive sediments. Aller (1980b) has developed an embedded interface model and showed that as the first step of irrigation, molecular diffusion dominates solute migration from the sediment to the burrow water. Advection ensues rapidly to flush solutes within the burrows into the overlying water. As a consequence, the concentration gradient near the wall of a burrow is reckoned the same with that at the surficial sediment-water interface (Aller, 1980b; Cai et al., 2014). The applicability of this method, known as the $^{224}Ra/^{228}Th$ disequilibrium approach, has recently been evaluated (Hong et al., 2018a).

In coarse, sandy sediments with a permeability greater than ~10^{-12}–10^{-11} m^2, shear flow-induced advective transport surpasses Brownian molecular diffusion and becomes the dominant process for solute exchange across the sediment-water interface (Huettel et al., 2014). Under such a circumstance, an advective transport model must be invoked to convert the ^{224}Ra flux into a flux estimate of the objective component. In terms of benthic flux of dissolved Fe, it is formulated as

$$F_{Fe} = F_{Ra} \cdot (\Delta Fe/\Delta Ra) \quad (3)$$

where the prefix Δ represents the concentration difference between bottom water and the porewater in the topmost sediment layer (Cook et al., 2018). In practice, both the concentration differences (ΔFe and ΔRa) and the concentration gradients ($\frac{\partial Fe}{\partial z}$ and $\frac{\partial Ra}{\partial z}$) were calculated from the measurements in the uppermost 0–1 cm porewater and in the bottom water. As such, the difference between the flux estimates derived from a diffusion based model and an advection based model is only 20%, which is solely caused by the inclusion of the term D_S^{Fe}/D_S^{Ra} in Eq. (2). Notably, this difference is generally smaller than the uncertainty associated with an individual estimate of benthic Fe flux (see Table 1).

With Eq. (2), we calculated benthic dissolved Fe fluxes. Because Fe concentration in bottom water was much smaller than that in porewater (Severmann et al., 2010; Zhang et al., in press), we assumed that bottom water Fe concentration was zero. Our calculations show that benthic fluxes of Fe changed essentially from zero to 89 mmol m^{-2} d^{-1}, with a median of 370 μmol m^{-2} d^{-1} (Table 1). The average uncertainty of all flux estimates listed in Table 1 is ~40%. In particular, high Fe fluxes are generally associated with

Table 1
Concentration gradients of dissolved ^{224}Ra ($\partial Ra/\partial z$) and Fe ($\partial Fe/\partial z$) at the sediment-water interface, and benthic fluxes ("+" upward) of ^{224}Ra (F_{Ra}) and Fe (F_{Fe}) in China coastal seas. Theoretical flux of Fe induced by molecular diffusion (F_M) and interfacial water exchange rate (υ) are also listed.

Station	Bottom Depth (m)	DO (μM)	F_{Ra} (dpm m^{-2} d^{-1})	$\partial Ra/\partial z$ (dpm cm^{-4})	$\partial Fe/\partial z$ (nmol cm^{-4})	F_{Fe} (μmol m^{-2} d^{-1})	F_M*	υ (m^3 m^{-2} d^{-1})
The northern South China Sea shelf and the adjacent Pearl River Estuary; August, 2012								
A1	9	108	6160 ± 760	0.024 ± 0.005	2.45	500 ± 130	6.4	0.52
A6	8	223	3960 ± 820	0.016 ± 0.001	0.32	62 ± 16	0.7	0.55
A11	14	226	400 ± 200	0.021 ± 0.005	3.43	51 ± 27	7.6	0.04
A16	42	180	160 ± 220	0.051 ± 0.005	0.76	2 ± 3	1.9	0.01
QD00	19	131	650 ± 260	0.025 ± 0.005	3.81	78 ± 34	8.2	0.05
QD04	47	152	670 ± 210	0.057 ± 0.007	166	1570 ± 530	437	0.02
QD10	34	150	560 ± 180	0.019 ± 0.004	163	3910 ± 1480	226	0.06
The Pearl River Estuary; November, 2013								
A01	20	167	5640 ± 1090	0.016 ± 0.003	16.1	4490 ± 1070	34	0.70
A03	7	196	6550 ± 660	0.022 ± 0.004	9.5	3100 ± 520	22	0.58
A04	8	187	6590 ± 870	0.027 ± 0.004	16.4	5110 ± 1000	21	0.49
A06	9	202	2020 ± 730	0.025 ± 0.003	172	10990 ± 3040	286	0.16
A09	26	208	2610 ± 590	0.037 ± 0.004	1.90	110 ± 30	3.2	0.14
The Pearl River Estuary; July, 2015†								
P03	5	79	540 ± 1110	0.008 ± 0.002	108	6200 ± 13000	260	0.14
A01	13	130	2010 ± 540	0.023 ± 0.004	10.0	700 ± 210	26	0.18
A03	11	102	−80 ± 670	0.065 ± 0.005	23.2	−20 ± 190	81	0.01
A04	13	110	2390 ± 580	0.059 ± 0.004	214	6900 ± 1700	600	0.08
A06	11	101	7810 ± 510	0.026 ± 0.004	115	27000 ± 4200	147	0.59
A09	23	129	3580 ± 430	0.081 ± 0.006	176	6100 ± 900	408	0.09
F401	33	93	9100 ± 530	0.044 ± 0.005	129	21000 ± 2600	378	0.41
The Jiulong River Estuary; January, 2014								
JL0	5	154	11700 ± 1100	0.006 ± 0.002	2.61	3800 ± 1050	5.8	2.0
JL1	3	230	12500 ± 1300	0.031 ± 0.006	10.3	3330 ± 760	22.8	0.81
JL2	4	235	4000 ± 790	0.012 ± 0.002	1.00	275 ± 70	2.7	0.56
JL3	6	242	2090 ± 820	0.036 ± 0.005	5.77	268 ± 70	9.8	0.12
JL5	8	240	720 ± 620	0.150 ± 0.010	1210	4730 ± 4030	2573	0.01
JL6	14	239	−470 ± 360	0.016 ± 0.004	6.59	−154 ± 125	19.7	0
JL7	16	243	1390 ± 230	0.048 ± 0.006	8.15	190 ± 38	17.7	0.06
The Jiulong River Estuary; August, 2014								
JL1	6	118	8910 ± 920	0.011 ± 0.004	143	89000 ± 29300	534	1.6
JL2	5	110	1370 ± 410	0.032 ± 0.006	377	13000 ± 4500	1330	0.09
JL3	5	183	1380 ± 490	0.112 ± 0.010	332	3220 ± 1180	1000	0.02
JL4	7	140	3120 ± 410	0.049 ± 0.006	400	21600 ± 4000	1440	0.13
JL5	8	194	830 ± 610	0.092 ± 0.008	1352	9570 ± 7040	4050	0.02
JL6	13	194	7960 ± 1160	0.089 ± 0.008	140	9770 ± 1660	262	0.18
JL7	12	190	1070 ± 220	0.060 ± 0.008	58	790 ± 200	132	0.04

Table 1 (*continued*)

Station	Bottom Depth (m)	DO (μM)	F_{Ra} (dpm m^{-2} d^{-1})	∂Ra/∂z (dpm cm^{-4})	∂Fe/∂z (nmol cm^{-4})	F_{Fe} (μmol m^{-2} d^{-1})	F_M *	υ (m^3 m^{-2} d^{-1})
The East China Sea shelf adjacent to the Yangtze River Estuary; August, 2017								
Y3	14	65	700 ± 40	0.014 ± 0.002	0.56	22 ± 3	2.0	0.10
Y4	17	116	990 ± 170	0.029 ± 0.002	126.	3450 ± 640	317	0.07
Y5	47	76	1040 ± 160	0.017 ± 0.001	3.62	180 ± 33	6.7	0.12
Y7	58	115	740 ± 190	0.015 ± 0.001	0.99	39 ± 10	1.5	0.10
E14	27	84	270 ± 55	0.040 ± 0.003	86.8	470 ± 100	247	0.01
E13	40	118	890 ± 110	0.030 ± 0.002	14.4	340 ± 50	33.8	0.06
E10	52	144	450 ± 170	0.011 ± 0.001	0.15	5 ± 2	0.3	0.08
E4	17	136	300 ± 180	0.029 ± 0.002	12.4	100 ± 60	27.1	0.02
E3	34	164	220 ± 85	0.015 ± 0.002	0.41	5 ± 2	1.3	0.03
The Yellow Sea and the Bohai Sea; June, 2016								
H05	52	120	−70 ± 450	0.027 ± 0.004	3.4	−7 ± 44	6.2	0
H11	77	80	−930 ± 600	0.048 ± 0.005	3.7	−57 ± 37	6.9	0
H31	33	72	70 ± 230	0.037 ± 0.004	6.4	9 ± 32	10.8	0
B05	29	148	2940 ± 340	0.044 ± 0.002	163	8670 ± 1410	207	0.13
BS4	64	132	2150 ± 390	0.053 ± 0.002	7.1	228 ± 47	9.5	0.08
B12	64	130	420 ± 250	0.068 ± 0.002	54.1	268 ± 160	41.9	0.01
B25	54	92	3050 ± 420	0.050 ± 0.001	46.7	2260 ± 360	76.7	0.12
B39	25	160	1190 ± 370	0.038 ± 0.001	14.3	362 ± 120	27.9	0.06
B43	23	115	1220 ± 340	0.044 ± 0.001	10.6	236 ± 70	21.1	0.06
B50	36	100	320 ± 300	0.047 ± 0.001	59.9	324 ± 303	92.4	0.01
B56	23	70	520 ± 290	0.051 ± 0.001	22.9	188 ± 107	31.9	0.02
B66	15	95	2770 ± 330	0.022 ± 0.001	7.1	713 ± 123	16.0	0.25

–: Data not available.

* The same unit of F_{Fe}.

† Data are from Hong et al. (2018a).

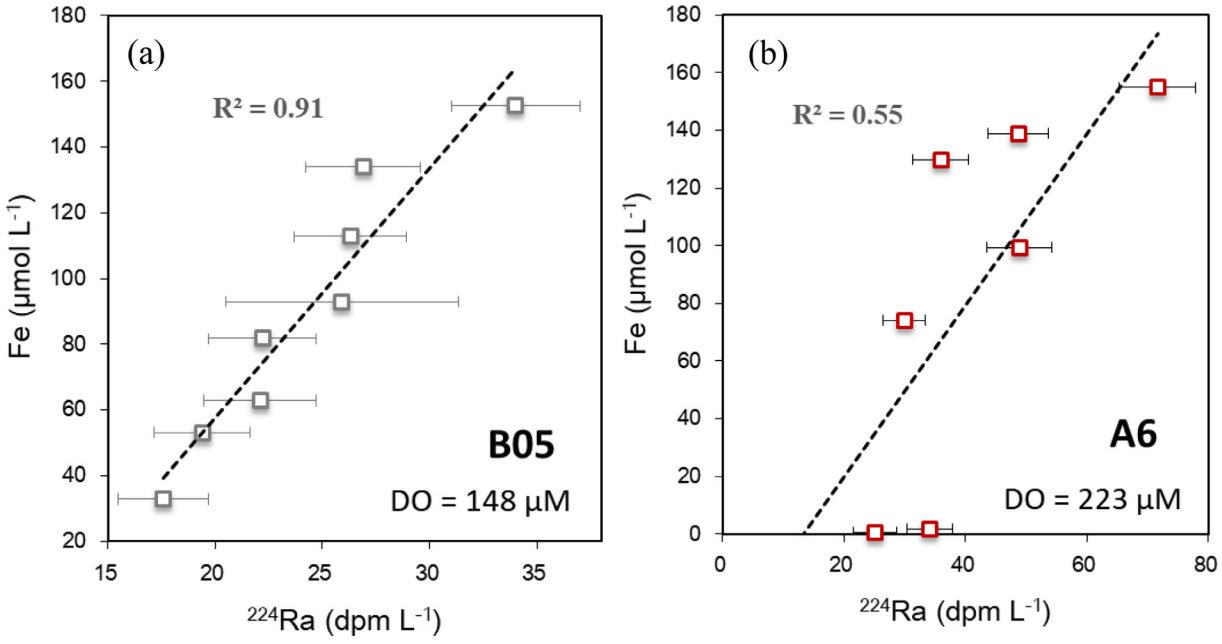

Fig. 3. Correlation of porewater ^{224}Ra (±1σ error) and Fe in the upper 0–10 cm sediment column at stations with different DO levels in the bottom water. The dashed line depicts the linear regression of the data.

relatively small errors of 10–30%. Notably, negative flux estimates commonly possess large uncertainties, which make these estimates essentially indistinguishable from zero. We compared flux calculations from two representative cases, e.g., St. A6 and B25. Despite that similar ^{224}Ra flux values were obtained at the two locations (3960 vs. 3050 dpm m^{-2} d^{-1}), the benthic flux of Fe at St. B25 was ~36 fold higher than that at St. A6 (2260 vs. 62 μmol m^{-2} d^{-1}, see Table 1). In the near-surface sediment, dissolved Fe(II) is readily impeded by oxygen that penetrates from the oxygenated overlying waters. As shown in Fig. 2, this process lowered the concentration gradient of dissolved Fe at the sediment-water interface. The comparison of Fe fluxes between St. A6 and B25 displays how the oxic layer in the surface sediment poses a barrier of rapid diffusion of dissolved Fe, and consequently greatly reduces the sediment-water transfer efficacy of Fe (Homoky et al., 2012). Although the concentration gradients of Fe across the sediment-water interface were more variable than ^{224}Ra (Table 1), we have identified a strong correlation of ^{224}Ra and Fe in porewater at St. B05 (Fig. 3a). This suggests that the difference between the geochemical behavior of ^{224}Ra and Fe might be small in the sediment at this location. In comparison, at St. A6 where bottom water was fully oxygenated, the correlation of ^{224}Ra and Fe in porewater is relatively poor (Fig. 3b).

4.2. Spatial variability in benthic Fe fluxes

Spatial and temporal variabilities in benthic Fe fluxes were large in China coastal seas. As compiled in Table 1, benthic Fe fluxes spanned over 4–5 orders of magnitude, from <10 μmol m^{-2} d^{-1} up to ~100 mmol m^{-2} d^{-1}. For a specific study region, like the Pearl River Estuary and the Jiulong River Estuary, there was no clear temporal pattern in benthic Fe fluxes. We have chosen to categorize all our Fe flux data based on bottom depth. While considerable variability is still evident at any 10-m depth interval, the average benthic Fe fluxes decline exponentially with bottom depth (Fig. 4a). This robust trend indicates that bottom depth is a first-order regulator of benthic Fe flux in the coastal seas. Notably, a recent investigation by utilization of ^{224}Ra/^{228}Th disequilibria showed similar large and highly variable fluxes of dissolved Fe in a tidal marshland of the southeastern United States, which ranged from 0.5 to 134 mmol m^{-2} d^{-1} (Shi et al., in press), but overall conformed to the trend that was identified from China coastal seas (Fig. 4a).

The magnitude of benthic Fe flux is determined ultimately by (1) how fast sediment porewater exchanges with overlying seawaters, and (2) how sharp the concentration gradient of dissolved Fe is at the sediment-water interface (Aller, 1980a). Fluid pressure fluctuations at the sediment-water interface can be induced by shear flow over the seafloor, causing overlying seawater to irrigate the sediment. In our prior studies, irrigation has been demonstrated to be the predominant mechanism for solute transfer across the sediment-water interface, and account for >90% of the total flux of ^{224}Ra into the coastal seas (Cai et al., 2015; Hong et al., 2017, 2018a). Irrigation is reckoned a process of interplay between small-scale advective flow and biological activities of infauna within the near-surface sediment. Fluid transport induced by irrigation can be simulated with an advection cycling model (Cook et al., 2018). This type of model consists of a series of vertically-stacked compartments. Water and solutes are assumed to be

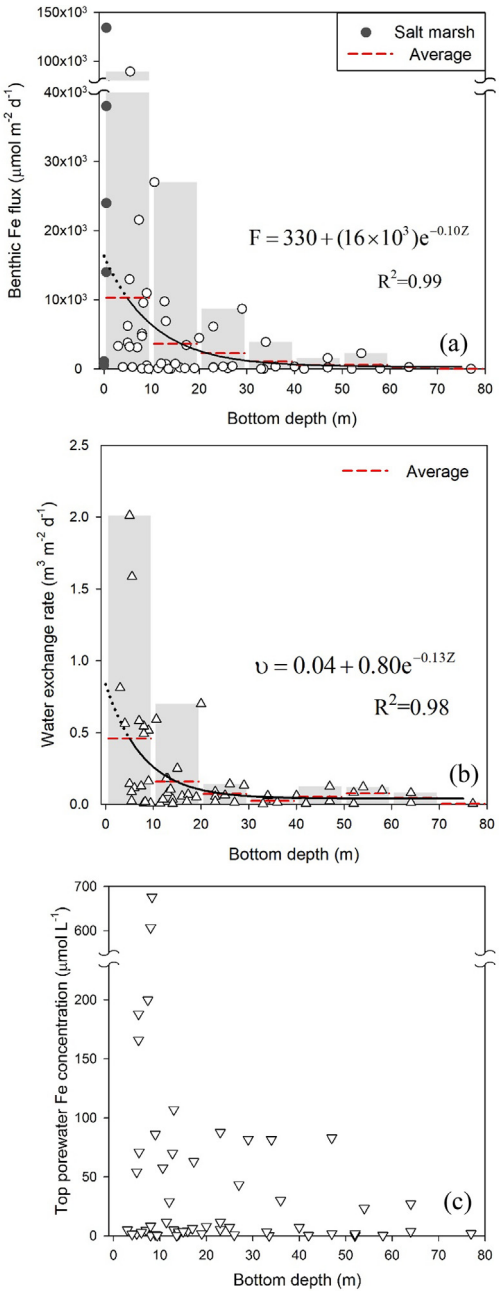

Fig. 4. The relationship between bottom depth and (a) benthic Fe flux in the China coastal seas (open circle). Solid circles represent Fe flux estimates collected from a salt marsh in the United States (Shi et al., in press); (b) water exchange rate across the sediment-water interface; (c) Fe concentration in the topmost porewater. The grey bars represent intervals of 10 m water depth, and the red dashed lines indicate the average value of each interval. The solid line stands for the regression of the interval averages (salt marsh data excluded). Note that negative flux values in Table 1 are replaced by molecular diffusive fluxes, which are used to represent a lower estimate of true benthic Fe fluxes. The data of St. F401 are excluded in the diagrams because this site is located in an uncommon convergence zone of regional summer flows (Lu et al., 2018). (For interpretation of the references to color in this figure legend, the reader is referred to the web version of this article.)

perfectly mixed within each compartment. Only advective transport between the compartments is explicitly considered. With this model, water flux across the sediment-water interface can be estimated from the deficit of ^{224}Ra in the sediment using

$$\upsilon = \frac{F_{Ra}}{\Delta Ra} \quad (4)$$

where υ stands for the interfacial water exchange rate (unit: $m^3\ m^{-2}\ d^{-1}$). As listed in Table 1, interfacial water exchange rates also exhibited considerable variabilities in China coastal seas. However, when all water flux data are sorted on the basis of a 10-m depth interval, a similar exponential attenuation of average water exchange rate with bottom depth is identified (Fig. 4b).

The attenuation of water flux across the sediment-water interface with bottom depth is in line with energy gradients that culminate in the coastal seas. The reduction in bottom depth toward the coast and ensuing compression of waves, tides, and currents convert potential into kinetic energy, resulting in enhanced turbulence, mixing, and shear flow over the seafloor. In the meantime, terrestrial input of organic matter via rivers and surface runoff creates peaks of chemically bound energy in the coastal seas. Consequently, benthic fauna that are fed by terrestrial organic matter flourish in estuaries and the inner shelves. Indeed, Middelburg et al. (2005) have noted that benthic respiration rates (R, unit: mmol C $m^{-2}\ d^{-1}$) in the continental shelf increase exponentially with decreasing bottom depth (Z) following a relationship $R = 32.1 \times e^{-0.0077 \times Z}$ ($Z < 300$ m). Intense biological activities of benthic fauna combined with enhanced shear flow over the seafloor would cause overlying seawater to flush the sediment more efficiently, thereby generating a gradient of interfacial water flux with depth as illustrated in Fig. 4b.

The concentration gradient of dissolved Fe across the sediment-water interface was also in step with the gradient of chemically bound energy in the coastal seas. As one of the most abundant elements in the earth's crust, Fe is rich in terrestrial materials. After deposition over the coastal seafloor, a fraction of reactive Fe oxides in sediment particles will be used as electron acceptors to decompose organic matter, leading to the release of soluble Fe(II). To a first approximation, dissolved Fe concentration in the topmost 0–1 cm porewater can be reckoned to mirror the level of reactive Fe that is released from sediment particles. It also reflects the concentration gradient at the sediment-water interface because in general, dissolved Fe concentration in overlying seawater is orders of magnitude lower than that in porewater. As shown in Fig. 4c, the offshore attenuation of porewater Fe concentration indicates that coastal sediments are a crucial source of reactive Fe. Although coastal seas comprise <8% of the total area of the global ocean, the sharp gradient of benthic Fe flux over bottom depth highlights the disproportionately important role of coastal sediments as a source of dissolved Fe (Fig. 4a).

In previous studies, benthic Fe fluxes were often assumed to increase with decreasing dissolved oxygen (DO) content in the bottom water because hypoxia conditions tend to shoal the oxygen penetration depth into the

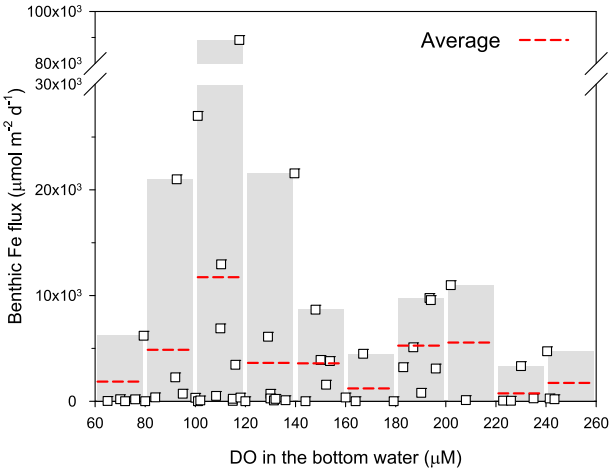

Fig. 5. The relationship between benthic Fe flux and dissolved oxygen (DO) concentration in the bottom water. The bars represent intervals of 20 μM DO concentration, and the dashed lines indicate the average Fe flux of each DO interval.

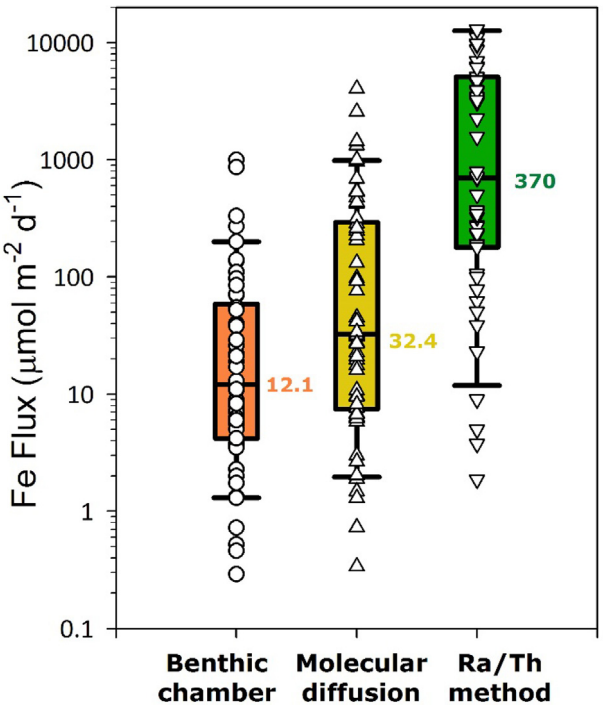

Fig. 6. Comparison of benthic Fe flux estimates derived from the $^{224}Ra/^{228}Th$ disequilibrium method with those derived from the porewater concentration gradient method (this study) and historical measurements based on the core incubation method (Table S6). Upper and lower boundaries of the boxes represent the 75th and 25th percentiles. Error bars above and below the boxes indicate the 90th and 10th percentiles. The lines within the boxes mark the medians (SigmaPlot 10.0).

sediment column, potentially allowing dissolved Fe in the sediment to migrate more efficiently into the overlying water column (Homoky et al., 2012). In contrast to this common assumption, our results show that in China coastal seas, high benthic Fe fluxes occurred more frequently within a redox window of 100–150 μM DO in the bottom water (Fig. 5). A plausible explanation of this phenomenon is that it reflects a compromise between irrigation and Fe re-oxidation on the transfer of dissolved Fe across the sediment-water interface. Although hypoxia alleviates the oxygen barrier of rapid diffusion of dissolved Fe, biologically-mediated irrigation is suppressed by the low levels of DO in the bottom water, which in turn tend to lower the transfer efficacy of dissolved Fe between the sediment and the overlying water. On the other way around, a fully oxic state over the seafloor boosts biologically-mediated irrigation, but its effect on Fe transfer could be counteracted by the DO-enhanced oxidative precipitation of Fe(III) in the near-surface sediment.

4.3. Comparison with benthic Fe fluxes derived from other methods

The traditional porewater concentration gradient method assesses Fe fluxes across the sediment-water interface solely induced by molecular diffusion using Fick's first law (Shaw et al., 1990):

$$F_M = \phi D_S^{Fe} \frac{\partial Fe}{\partial z} \quad (5)$$

In the above expression, the term D_S^{Fe} is computed from the molecular diffusion coefficient for Fe(II) (D^{Fe}) in seawater using the relation $D_S^{Fe} = D^{Fe}/\theta^2$, where θ denotes the sediment tortuosity and is derived from the porosity (ϕ) using the expression $\theta^2 = 1 - 2\ln(\phi)$ (Boudreau, 1996). Benthic fluxes of Fe based on this method (F_M) ranged from 0.7 to 4050 μmol m^{-2} d^{-1}, with a median of 32.4 μmol m^{-2} d^{-1} (Table 1 and Fig. 6). On average, the benthic flux estimates of Fe based on the $^{224}Ra/^{228}Th$ disequilibrium approach were one order of magnitude higher than those derived from the porewater concentration gradient method. This discrepancy is most likely due to the fact that the latter does not incorporate a major process that regulates solute exchange across the sediment-water interface, i.e., irrigation. Its importance has been well elucidated in a series of previous studies (Cai et al., 2014, 2015).

Another traditional way of assessing benthic fluxes of Fe is to use a core incubation method (Elrod et al., 2004). An analysis of historical measurements in the global coastal seas based on this method outlines a wide range of Fe fluxes, which changed from <0.02 to ~1000 μmol m^{-2} d^{-1} (median Fe flux: 12.1 μmol m^{-2} d^{-1}) (Fig. 6 and Table S6). Overall, our estimates of benthic Fe flux derived from $^{224}Ra/^{228}Th$ disequilibria are ~30 times higher than the median flux value based on the incubation method (370 vs. 12.1 μmol m^{-2} d^{-1}). This discrepancy is likely linked to the limitations inherent in the core incubation method.

There are at least two fundamental problems with the core incubation method: (1) it does not realistically mimic the hydrodynamics that can cause transport rates to be several times higher than diffusive fluxes across the surficial sediment-water interface (Reimers et al., 2001). Indeed, recently a compilation of ^{224}Ra fluxes derived from core incubation experiments and from the $^{224}Ra/^{228}Th$

disequilibrium approach revealed that the core incubation method underestimates true benthic solute fluxes by more than one order of magnitude (Hong et al., 2018b); (2) it assumes that aside from the sediment-water exchange, there is no removal or addition of the objective component from and to the chamber water during core incubation experiments. More specifically, the general formula to describe changes of solute concentration with time ($\frac{dc}{dt}$) in chamber water is

$$\frac{dc}{dt} = \frac{FA}{V} + \Sigma R \quad (6)$$

where F is the benthic flux of a solute from bottom sediments; A is the surface area of the sediment within the chamber; V is the volume of overlying water trapped within the chamber; and ΣR denotes all the reaction terms that add (a "+" R term) or remove (a "–" R term) the solute of interest to and from the chamber water. If, and only if $\Sigma R = 0$, the above expression can be simplified to the form of $\frac{dc}{dt} = \frac{FA}{V}$ (e.g., Reimers et al., 2001). For Fe, this assumption is unlikely to be valid because under the typical seawater condition, Fe(II) can be rapidly oxidized into Fe(III) and subsequently be precipitated on the chamber walls, the suspended particles, the sediment surface, or within the sample vials prior to filtration (Severmann et al., 2010). Similar problems have been identified in a core incubation experiment for Hg, a redox sensitive metal like Fe (Shi et al., 2018). Moreover, the half-life of dissolved Fe (II), which describes the rate of Fe(II) loss through oxidation, is on the order of a few hours under the typical upper ocean condition (Lohan and Bruland, 2008). This time scale is considerably shorter than the common incubation time of 1–2 days. It is thus expected that a major portion of dissolved Fe would be removed from the chamber water over the duration of benthic incubation experiments. Consequently, benthic fluxes of Fe could be greatly underestimated by the core incubation method. Indeed, when Fe loss through oxidation was taken into account, model results gave benthic Fe fluxes of 1000 and 3000 μmol $m^{-2}\,d^{-1}$ in the Oregon-California continental shelf (Severmann et al., 2010). This value is 1–2 orders of magnitude higher than the benthic fluxes derived from the incubation method (17 and 332 μmol $m^{-2}\,d^{-1}$), but is compatible with our $^{224}Ra/^{228}Th$-based flux estimates in the China coastal seas.

In the recent years, a new two dimensional (2D) imaging technique was developed to estimate benthic flux of dissolved Fe across the sediment-water interface. This technique is based on the numerical analyses of high resolution (200 μm) 2D images of dissolved Fe in coastal sediments (Thibault de Chanvalon et al., 2017). Unlike the one dimensional porewater concentration gradient method, the 2D imaging technique permits to estimate both the diffusive flux across the surficial sediment-water interface and the irrigational flux. An application of this technique to an intertidal mudflat densely inhabited by macrofauna revealed that the irrigational flux accounted for up to 80% of the total benthic Fe flux of 514 ± 233 μmol $m^{-2}\,d^{-1}$ (Thibault de Chanvalon et al., 2017). This finding is in general agreement with our results based on the $^{224}Ra/^{228}Th$ disequilibrium approach.

We must emphasize that like the porewater concentration gradient method and the 2D imaging method, the $^{224}Ra/^{228}Th$ disequilibrium approach provides benthic dissolved Fe fluxes across the sediment-water interface. Immediately out of the sediment-water interface, a fraction of highly soluble Fe(II) released from the near-surface sediment layer may be oxidized to particle reactive Fe(III), and subsequently be precipitated at the top of the sediment pile, thereby lowering the true dissolved Fe flux into the water column. In this sense, the benthic Fe fluxes based on $^{224}Ra/^{228}Th$ disequilibria essentially reflect a potential for sediments to supply dissolved Fe to overlying waters. Quantification of subsequent transport of Fe (either in the dissolved phase or in the solid phase) from the Benthic Nepheloid Layer (BNL) into the upper water column, and finally across the continental shelf-open ocean boundary is thus critically important for understanding the role of coastal sediments in the global ocean Fe cycle (Charette et al., 2016; Sanial et al., 2018). In this respect, complexation by high levels of organic ligands generated in surface sediments and re-suspension of Fe-enriched fine sediment particles could sustain Fe in the water column, and may facilitate its long-range transport from coastal seas into the deep ocean (Nishioka and Obata, 2017). Mechanisms controlling the transport efficiency of Fe between the coastal sea and the open ocean should be dived into in future studies.

5. SUMMARY

We utilized the $^{224}Ra/^{228}Th$ disequilibrium method to estimate benthic flux of dissolved Fe in China coastal seas, and unveiled large spatial and temporal variabilities in benthic Fe fluxes. In a stepwise manner, however, the benthic Fe fluxes exhibit an exponential decrease with bottom depth. We also illustrated that large Fe fluxes frequently occur within a narrow redox window of 100–150 μM dissolved oxygen in the bottom water. Furthermore, our estimates are 1–2 orders of magnitude higher than historical measurements based on the traditional methods, but in general agreement with the Fe flux depicted from a new 2D imaging technique. Overall, this study suggests that the potential of coastal sediments as a source of dissolved Fe could be much larger than previously thought.

ACKNOWLEDGEMENTS

This work was supported by the Natural Science Foundation of China (NSFC) through Grants No. 41776083 and by the National Major Science and Technology Projects of China through Grants No. 2016YFC0300709 and 2015CB954003. The authors thank the crew of R/V *Dongfanghong II* for the assistance in sampling, and Ms. Pingping Mi for the logistics support.

APPENDIX A. SUPPLEMENTARY MATERIAL

Supplementary data to this article can be found online at https://doi.org/10.1016/j.gca.2019.06.026.

REFERENCES

Aller R. C. (1980a) Diagenetic processes near the sediment-water interface of long island sound. II.: Fe and Mn. *Adv. Geophys.* **22**, 351–415.

Aller R. C. (1980b) Quantifying solute distributions in the bioturbated zone of marine sediments by defining an average microenvironment. *Geochim. Cosmochim. Acta* **44**, 1955–1965.

Berner R. A. (1980) *Early eiagenesis-A theoretical approach*. Princeton Unversity Press, New Jersey, p. 334.

Boudreau B. P. (1996) The diffusive tortuosity of fine-grained unlithified sediments. *Geochim. Cosmochim. Acta* **60**, 3139–3142.

Boyd P. W. and Ellwood M. J. (2010) The biogeochemical cycle of iron in the ocean. *Nat. Geosci.* **3**, 675–682.

Cai P., Shi X., Moore W. S. and Dai M. (2012) Measurement of Ra-224: Th-228 disequilibrium in coastal sediments using a delayed coincidence counter. *Mar. Chem.* **138**, 1–6.

Cai P., Shi X., Moore W. S., Peng S., Wang G. and Dai M. (2014) ^{224}Ra:^{228}Th disequilibrium in coastal sediments: Implications for solute transfer across the sediment-water interface. *Geochim. Cosmochim. Acta* **125**, 68–84.

Cai P., Shi X., Hong Q., Li Q., Liu L., Guo X. and Dai M. (2015) Using ^{224}Ra/^{228}Th disequilibrium to quantify benthic fluxes of dissolved inorganic carbon and nutrients into the Pearl River Estuary. *Geochim. Cosmochim. Acta* **170**, 188–203.

Charette M. A., Lam P. J., Lohan M. C., Kwon E. Y., Hatje V., Jeandel C., Shiller A. M., Cutter G. A., Thomas A., Boyd P. W., Homoky W. B., Milne A., Thomas H., Andersson P. S., Porcelli D., Tanaka T., Geibert W., Dehairs F. and Garcia-Orellana J. (2016) Coastal ocean and shelf-sea biogeochemical cycling of trace elements and isotopes: lessons learned from GEOTRACES. *Phil. Trans. R. Soc. A* **374**, 20160076.

Conway T. M. and John S. G. (2014) Quantification of dissolved iron sources to the North Atlantic Ocean. *Nature* **511**, 212–215.

Cook P. G., Rodellas V., Andrisoa A. and Stieglitz T. C. (2018) Exchange across the sediment-water interface quantified from porewater radon profiles. *J. Hydrol.* **559**, 873–883.

de Baar H. J. W., de Jong J. T. M., Bakker D. C. E., Loscher B. M., Veth C., Bathmann U. and Smetacek V. (1995) Importance of iron for plankton blooms and carbon dioxide drawdown in the Southern Ocean. *Nature* **373**, 412–415.

Elrod V. A., Berelson W. M., Coale K. H. and Johnson K. S. (2004) The flux of iron from continental shelf sediments: A missing source for global budgets. *Geophys. Res. Lett.* **31**, L12307.

He M. H., Cai E. X., Wu Q. Q., Jiang J. X., Lin S. D., Xu H. Z., Liu Q. S., Zheng F. W. and Li R. G. (1988) Studies on the ecology of benthos in the Jiulong Jiang Estuary (In Chinese with English Abstract). *Acta Ecol. Sin.* **8**, 133–139.

Homoky W. B., Severmann S., McManus J., Berelson W. M., Riedel T. E., Statham P. J. and Mills R. A. (2012) Dissolved oxygen and suspended particles regulate the benthic flux of iron from continental margins. *Mar. Chem.* **134**, 59–70.

Hong Q., Cai P., Shi X., Li Q. and Wang G. (2017) Solute transport into the Jiulong River estuary via pore water exchange and submarine groundwater discharge: New insights from ^{224}Ra/^{228}Th disequilibrium. *Geochim. Cosmochim. Acta* **198**, 338–359.

Hong Q., Cai P., Geibert W., Cao Z., Stimac I., Liu L. and Li Q. (2018a) Benthic fluxes of metals into the Pearl River Estuary based on ^{224}Ra/^{228}Th disequilibrium: From alkaline earth (Ba) to redox sensitive elements (U, Mn, Fe). *Geochim. Cosmochim. Acta* **237**, 223–239.

Hong Q., Shi X., Wei L., Cai P. and Mi P. (2018b) Progresses and outlooks of the research on solute exchange across the sediment-water interface using a novel ^{224}Ra/^{228}Th disequilibrium approach. *Bull. Mineral. Petrol. Geochem.* **37**, 827–840 (in Chinese with English Abstract).

Huettel M., Berg P. and Kostka J. E. (2014) Benthic exchange and biogeochemical cycling in permeable sediments. *Annu. Rev. Mar. Sci.* **6**, 23–51.

Jeandel C., Peucker-Ehrenbrink B., Jones M. T., Pearce C. R., Oelkers E. H., Godderis Y., Lacan F., Aumont O. and Arsouze T. (2011) Ocean margins: The missing term in oceanic element budgets? *Eos* **92**, 217–218.

Kolber Z. S., Barber R. T., Coale K. H., Fitzwateri S. E., Greene R. M., Johnson K. S., Lindley S. and Falkowski P. G. (1994) Iron limitation of phytoplankton photosynthesis in the equatorial Pacific Ocean. *Nature* **371**, 145–149.

Lam P. J. and Bishop J. K. B. (2008) The continental margin is a key source of iron to the HNLC North Pacific Ocean. *Geophys. Res. Lett.* **35**, 521–539.

Li K. Z., Yin J. Q., Huang L. M., Lian S. M., Zhang J. L. and Liu C. G. (2010) Monsoon-forced distribution and assemblages of appendicularians in the northwestern coastal waters of South China Sea. *Estuar. Coast Shelf Sci.* **89**, 145–153.

Liu X., Fan Y., Shi S., Hua E. and Zhang Z. (2014) *Studies on the species composition and community structure of macrofauna in the Bohai Sea*. Acta Oceanologica Sinica, China (in Chinese).

Lohan M. C. and Bruland K. W. (2008) Elevated Fe(II) and dissolved Fe in hypoxic shelf waters off Oregon and Washington: An enhanced source of iron to coastal upwelling regimes. *Environ. Sci. Technol.* **42**, 6462–6468.

Lu Z., Gan J., Dai M., Liu H. and Zhao X. (2018) Joint effects of extrinsic biophysical fluxes and intrinsic hydrodynamics on the formation of hypoxia west off the Pearl River Estuary. *J. Geophys Res. Oceans* **123**, 6241–6259.

Martin J. H. (1990) Glacial-interglacial CO_2 change: The iron hypothesis. *Paleoceanogr.* **5**, 1–13.

Martin J. H. and Gordon R. M. (1988) Northeast Pacific iron distributions in relation to phytoplankton productivity. *Deep Sea Res. Part A* **35**, 177–196.

Middelburg J. J., Duarte C. M. and Gattuso J.-P. (2005) Respiration in coastal benthic communities. In *Respiration in Aquatic Ecosystems* (eds. P. A. D. Giorgio and P. J. B. Williams). Oxford University Press, New York, pp. 206–224.

Moore C. M., Mills M. M., Achterberg E. P., Geider R. J., Laroche J., Lucas M. I., Mcdonagh E. L., Pan X., Poulton A. J. and Rijkenberg M. J. A. (2009) Large-scale distribution of Atlantic nitrogen fixation controlled by iron availability. *Nat. Geosci.* **2**, 867–871.

Nishioka J. and Obata H. (2017) Dissolved iron distribution in the western and central subarctic Pacific: HNLC water formation and biogeochemical processes. *Limnol. Oceanogr.* **62**, 2004–2022.

Reimers C., Jahnke R. and Thomsen L. (2001) In situ sampling in the benthic boundary layer. In *In the benthic boundary layer: Transport processes and biogeochemistry* (eds. B. P. Boudreau and B. B. Jørgensen). Oxford University Press, New York, pp. 72–80.

Sanial V., Kipp L. E., Henderson P. B., van Beek P., Reyss J. L., Hammond D. E., Hawco N. J., Saito M. A., Resing J. A., Sedwick P., Moore W. S. and Charette M. A. (2018) Radium-228 as a tracer of dissolved trace element inputs from the Peruvian continental margin. *Mar. Chem.* **201**, 20–34.

Schulz H. (2006) Quantification of early diagenesis: Dissolved constituents in pore water and signals in the solid phase. In *Marine Geochemistry* (eds. H. D. Schulz and M. Zabel). Springer, Heidelberg, pp. 73–124.

Seeberg-Elverfeldt J., Schluter M., Feseker T. and Kolling M. (2005) Rhizon sampling of porewaters near the sediment-water

interface of aquatic systems. *Limnol. Oceanogr. Methods* **3**, 361–371.

Severmann S., McManus J., Berelson W. M. and Hammond D. E. (2010) The continental shelf benthic iron flux and its isotope composition. *Geochim. Cosmochim. Acta* **74**, 3984–4004.

Shaw T. J., Gieskes J. M. and Jahnke R. A. (1990) Early diagenesis in differing depositional environments: The response of transition metals in pore water. *Geochim. Cosmochim. Acta* **54**, 1233–1246.

Shi X., Benitez-Nelson C. R., Cai P., He L. and Moore W. S. (in press) Development of a two-layer transport model in layered muddy–permeable marsh sediments using ^{224}Ra–^{228}Th disequilibria. *Limnol. Oceanogr.*. https://doi.org/10.1002/lno.11143 (in press).

Shi X., Mason R. P., Charette M. A., Mazrui N. M. and Cai P. (2018) Mercury flux from salt marsh sediments: Insights from a comparison between ^{224}Ra/^{228}Th disequilibrium and core incubation methods. *Geochim. Cosmochim. Acta* **222**, 569–583.

Sigman D. M. and Boyle E. A. (2000) Glacial/interglacial variations in atmospheric carbon dioxide. *Nature* **407**, 859–869.

Thibault de Chanvalon A., Metzger E., Mouret A., Knoery J., Geslin E. and Meysman F. J. R. (2017) Two dimensional mapping of iron release in marine sediments at submillimetre scale. *Mar. Chem.* **191**, 34–49.

Zhang R., Zhu X., Yang C., Ye L., Zhang G., Ren J., Wu Y., Liu S., Zhang J. and Zhou M. (in press) Distribution of dissolved iron in the Pearl River (Zhujiang) Estuary and the northern continental slope of the South China Sea. *Deep Sea Res. Part II*. https://doi.org/10.1016/j.dsr2.2018.12.006 (in press).

Associate editor: Claudine Stirling